

Correcting the Geometry and Color of Digital Images

M. Jackowski, A. Goshtasby, *Senior Member, IEEE*,
S. Bines, D. Roseman, and C. Yu

Abstract—A unified method for correcting the geometry and color of digital images is presented. The method uses a color chart with a prearranged array of known color patches. Using the true geometry and color of the chart and geometry and color of the image of the chart, transformation functions that describe the geometry and color characteristics of the camera are determined. The transformation functions are then used to correct the geometry and color of obtained images. Experimental results of the proposed method on images acquired under different scene illuminations and camera settings are presented and evaluated.

Index Terms—Geometry correction, color correction, approximation, parametric surface, rational Gaussian surface.

1 INTRODUCTION

A digital image is a projection of a scene onto a plane after being digitized into discrete pixel positions and intensities. A vision system uses the positions and intensities of the pixels to interpret the scene. Inaccuracies in pixel positions and intensities will mislead the vision system; therefore, it is crucial that an image's geometry and color are corrected before it is analyzed.

Geometry and color distortions in an image can be the result of camera or environmental factors. A camera's sensor may displace red, green, and blue color values, and an imperfect lens may displace the image pixels from their true positions. Inhomogeneous scene illumination or use of a nonwhite light will change true scene colors, and atmospheric turbulence will displace image pixels from their true positions. Chromatic aberration in a camera's lens projects the three color bands differently, causing misregistration between the bands and distortion of image colors.

To correct the geometry and color of images acquired by a camera, an image of a scene whose geometry and color are known is obtained. Then, two sets of transformation functions are determined: one set relating the ideal image geometry to the obtained image geometry, and another set relating the true colors in the scene to colors in the image of the scene. These transformation functions are then used to correct the geometry and color of subsequently acquired images.

The position of a pixel in an image is represented by its x and y coordinates, while the color of a pixel is represented by its *red*, *green*, and *blue* values. Two transformation functions are, therefore, needed to correct an image's geometry, while three transformation functions are needed to correct an image's color. Since these transformation functions represent distortions introduced by both the camera and the environment, new transformation functions have

to be determined every time the parameters of either the camera or the environment are changed.

In many vision applications, it is necessary to standardize an image to a theoretical image obtained by a known camera system and under a known scene illumination. We will describe our procedure, assuming that the parameters of the camera and scene illumination are fixed and only the contents of the scene change from one image to another. For applications where the parameters of the camera and/or scene illumination change from one image to another, the procedure described here should be repeated at a number of camera and illumination settings. The parameters of the transformation functions that correct the geometry and color of a particular setting of the camera and illumination can then be estimated from the parameters of the transformation functions that correct the geometry and color of images obtained at known settings of the camera and scene illumination. Willson [42] discusses this procedure in detail.

In the following, existing geometry and color correction techniques are reviewed in Section 2, and a unified method for standardizing the geometry and color of digital images is introduced in Sections 3 and 4. Experimental results evaluating the proposed method are presented in Section 5, and concluding remarks are made in Section 6.

2 BACKGROUND

Many image analysis programs use the positions of image features to make decisions. In these programs, it is crucial that obtained images are corrected for geometric distortions. Image geometric distortions result from lens nonlinearities [36], sensor nonlinearities [11], or environmental factors such as atmospheric turbulence. Image distortions from lens nonlinearities result from a lens's radial and/or tangential distortions [5]. A lens's radial distortion causes image points to displace from their true positions towards or away from the image center, while a lens's tangential distortion causes image points to be displaced in the direction perpendicular to the line connecting them to the image center. A straight line passing through the image center will stay straight (although it may stretch or shrink) under the radial distortion, but the same straight line will become curved under the tangential distortion. Radial distortion results from imperfect lens design, while tangential distortion results from decentering of the lens elements during manufacturing of the lens.

Methods for correcting image geometric distortions already exist in the literature. Green et al. [11] used composite affine transformations, while Goshtasby [7] used Bézier patches to correct image distortions. Tsai [37], Lenz and Tsai [24], and Weng et al. [41] used iterative methods for correcting image distortions from lens nonlinearities. Since lens distortions cause straight lines in a scene map to curves in obtained images, Echigo [4] and Wang and Tsai [40] used this property to correct image geometric distortions. These methods are global, and, although they can compensate for lens distortions well, they cannot accurately model sharp distortions from sensor nonlinearities and atmospheric turbulences. A method is introduced in this paper that uses elastic transformation functions to represent a wide range of geometric distortions in an image.

Many vision systems use color as a feature for object recognition. For instance, spectral information in multiband aerial or satellite images has been used to classify image regions into roads, vegetation, and water [28]. Although surface colors can be characterized independent of scene illumination [1], [13], [25], many algorithms depend on absolute image colors that are influenced by scene illumination [34]. Vision systems that use absolute image colors in decision making lose their effectiveness when either a scene's illumination is changed or a camera's sensor inaccurately

• M. Jackowski and A. Goshtasby are with the Department of Computer Science and Engineering, Wright State University, Dayton, OH 45435. E-mail: {mjack, agoshtas}@cs.wright.edu.

• S. Bines and D. Roseman are with the Department of General Surgery, Rush-Presbyterian-St. Luke's Medical Center, Chicago, IL 60612. E-mail: sbines@rush.edu, dlr@oceana.net.

• C. Yu is with the Department of Electrical Engineering and Computer Science, University of Illinois at Chicago, Chicago, IL 60607. E-mail: yu@eecs.uic.edu.

Manuscript received 1 Apr. 1996. Recommended for acceptance by S.K. Nayar. For information on obtaining reprints of this article, please send e-mail to: tpami@computer.org, and reference IEEECS Log Number 105508.

records colors. To improve the accuracy of such systems, the colors in acquired images should be corrected before use.

Attempts to correct image colors have been made before. Existing methods can be categorized into

- 1) white-point mapping,
- 2) illumination estimation, and
- 3) lookup tables.

White-point mapping involves forcing the white point of the recorded image to the ideal white point. In this method, typically, a white reference card is imaged and the value at each band is adjusted in such a way that all three bands have the same value [33]. In the illumination estimation method, the chromaticity of the scene illumination is determined either directly or indirectly and used to correct image color. Lee [23] describes a method for estimating the scene illumination using specular highlight of the surface reflections. Knowing the spectral reflectances, Vrhel and Trussell [38] developed a method to correct image colors based on principal-components analysis.

In the lookup table approach for color correction, a table is prepared that contains, for a number of image colors, corresponding true colors. If a color that is being reproduced is not in the lookup table, it is estimated by interpolating or approximating the colors in the table [16], [19]. The method introduced in this paper can be categorized as a lookup table method, although no lookup tables are explicitly created. We determine three transformation functions, using a number of image colors whose true values are known. The transformation functions are then used to estimate, for each color in an image, its true color.

The choice of transformation functions plays a major role in the color-correction accuracy. If the color characteristics of the input and output are known, suitable transformation functions can be selected. However, because such information usually is not available, the selected transformation functions should represent a wide range of color distortions.

Hung [16], [17] and Kang [20] used polynomials to relate acquired colors to the desired one. Polynomials are global functions and will spread local distortions over the entire color space. Input and output devices that possess sharp nonlinearities require locally sensitive functions that can represent such high variations. Kang and Anderson [21] used neural networks to model the transformation functions for color correction and reported improved accuracy over the polynomial method. Transformation functions that use information about the physical characteristics of the input and output devices have also been used [2], [14], [15].

A method proposed by Kanamori et al. [18] determines a digital approximation to the transformation functions, using a grid of $9 \times 9 \times 9$ uniformly spaced colors. For acquired colors falling on grid points, the true colors are immediately obtained from the table. For acquired colors not falling on grid points, true colors are estimated by interpolating the true colors at the vertices of a tetrahedron containing the color under consideration. This technique can represent an input or output device's color characteristics well, but it requires the use of nine color charts, each containing an array of 9×9 color patches.

Color distortions occur if the three color bands in an image have slight geometric differences [42]. Usually, a color picture is obtained with a single lens by alternately placing three bandpass filters in the optical path of the camera and obtaining three images with the same lens. Color distortion from chromatic aberration results from the fact that the index of refraction of the lens varies as a function of the wavelength. The difference in indices of refraction from different colors causes different wavelengths of light to be bent by different amounts. For instance, a thin lens with incident white light will cause the blue component to focus closer to the lens than the red component will [42]. Therefore, to eliminate

or reduce the geometric difference between the bands in a color image, we will first correct the geometry of the three color bands independently, and then correct the image colors.

We will use elastic transformation functions in this paper. Elastic transformation functions are locally sensitive and adapt well to the local geometry and color characteristics of an image-acquisition system. By varying the elasticity of the functions, a wide range of geometry and color distortions can be modeled.

3 GEOMETRY CORRECTION

To correct the geometry of an image, a known grid is placed in front of the camera and its image is obtained. Because the geometry of the grid is known, the distortion at the grid points can be measured using the coordinates of corresponding grid points in the ideal and obtained images. At nongrid points, the distortions are estimated from the distortions at the grid points.

Assuming grid point (X_i, Y_i) in the distorted image corresponds to grid point (x_i, y_i) in the ideal image, for $i = 1, \dots, N$, we have to determine two functions f_x and f_y such that

$$x_i \approx f_x(X_i, Y_i), \quad (1)$$

$$y_i \approx f_y(X_i, Y_i), \quad i = 1, \dots, N. \quad (2)$$

If we arrange the coordinates of corresponding ideal and obtained grid points into two sets of 3D points as follows:

$$\{(X_i, Y_i, x_i) : i = 1, \dots, N\}, \quad (3)$$

$$\{(X_i, Y_i, y_i) : i = 1, \dots, N\}, \quad (4)$$

we can then consider f_x and f_y as two surfaces fitting the 3D point sets shown in (3) and (4), respectively. Note that, if points were uniformly spaced, we could have used tensor-product surfaces such as the B-splines to represent the transformation functions. But, because of the image noise, not all grid points can be determined; therefore, the available grid points may be irregularly spaced. Radial basis functions [31] can be used, but they require solution of a system of equations. In the following, we will use rational Gaussian surfaces that, like B-splines, are immediately obtained by substituting the coordinates of the grid points into the equation of the surface without solving a system of equations. But, unlike B-splines, rational Gaussian surfaces can fit to irregularly spaced points and are elastic. By varying the elasticity of a rational Gaussian surface, the tightness of the fit can be controlled.

Rational Gaussian surfaces have been introduced in [8]. The standard deviation of the Gaussians in this representation determines the stiffness (inverse elasticity) of the obtained surface. The smaller the standard deviation, the more elastic the surface, thus approximating the measurements more closely. Too small a standard deviation, however, will generate a surface that is similar to a piecewise linear approximation [8] and will treat noise in the measurements as image deformations, while too large a standard deviation will smooth out local details and produce surfaces that cannot represent sharp image deformations. If the image coordinates are normalized such that they are between 0.0 and 1.0, the standard deviations are typically between 0.01 and 0.1. For the images used in this paper, best accuracy was achieved when a standard deviation equal to 0.05 was used. The optimal standard deviation depends both on the magnitude of noise and on the sharpness of geometric distortions in an image. The best standard deviation for geometry correction of images obtained by a camera can be experimentally determined by using a few of the images and comparing the obtained errors at a variety of standard deviations.

4 COLOR CORRECTION

To correct the colors of images obtained by a camera, a known color chart is placed in front of the camera and its image is obtained. If the true colors in the chart and their correspondences in

the image are known, then three transformation functions can be determined to relate the three color components in the chart to the corresponding color components in the image of the chart.

Let us assume that the camera records colors in red, green, and blue, and the chart contains N homogeneous color patches. Also, suppose $\{(r_i, g_i, b_i) : i = 1, \dots, N\}$ represents the true colors in a chart and $\{(R_i, G_i, B_i) : i = 1, \dots, N\}$ represents corresponding colors recorded in the image of the chart. We need three transformation functions that can map the three components of colors in the image to the three color components in the chart. Denoting the three transformation functions by f_r, f_g , and f_b , the functions should satisfy

$$r_i \approx f_r(R_i, G_i, B_i), \quad (5)$$

$$g_i \approx f_g(R_i, G_i, B_i), \quad (6)$$

$$b_i \approx f_b(R_i, G_i, B_i), \quad i = 1, \dots, N. \quad (7)$$

If we arrange the true and obtained color coordinates into three sets of 4D points as follows:

$$\{(R_i, G_i, B_i, r_i) : i = 1, \dots, N\}, \quad (8)$$

$$\{(R_i, G_i, B_i, g_i) : i = 1, \dots, N\}, \quad (9)$$

$$\{(R_i, G_i, B_i, b_i) : i = 1, \dots, N\}, \quad (10)$$

we can consider f_r, f_g , and f_b as three hypersurfaces fitting to the 4D point sets given by (8), (9), and (10), respectively. Functions exist in literature that can represent f_r, f_g , and f_b . For instance, splines [3], sum of Gaussians [9], multiquadrics [12], and other radial basis functions [31] can represent the three transformation functions, and the parameters of the functions can be determined by solving three systems of linear equations.

If colors in the chart form a regular grid in the color space, then tensor-product functions, such as the B-splines [32], can be used to represent the functions without solving a system of equations. However, generating color charts that contain uniformly spaced colors is a difficult task. If we use commercially available charts that contain nonuniformly spaced colors [27], we need functions that can fit to irregularly spaced points. Each transformation function to be found here is a 4D hypersurface that corrects one band of an acquired color image using information about all bands of the ideal image.

In this paper, rational Gaussian hypersurfaces will be used to represent the transformation functions for color correction. A rational Gaussian hypersurface in 4D is an extension of a rational Gaussian surface in 3D [8], [10] and is obtained by replacing the 2D Gaussians with 3D Gaussians.

The standard deviation of the Gaussians in the proposed representation determines the smoothness of the obtained hypersurface. The smaller the standard deviation, the more elastic the hypersurface, better representing local variations in the color characteristics of the camera. The larger the standard deviation, the less elastic the hypersurface, representing a smoothly varying color distortion. As the standard deviation of Gaussians becomes smaller, a rational Gaussian surface approaches a piecewise linear function [8], [10]. If the color coordinates are normalized to vary between 0.0 and 1.0, the standard deviation of Gaussians may be varied between 0.01 and 0.1. A value smaller than 0.01 will make the hypersurface too elastic, responding to noise in the measurements, while a value larger than 0.1 will make the hypersurface too stiff, incapable of representing sharp variations in the color characteristics of the camera. For images used in this paper, we experimentally found that the standard deviation of Gaussians equal to 0.025 produces the best results.

Parkkinen et al. [30] found that scanner responses can be accurately represented by a linear combination of a number of basis functions. A procedure developed by Marimont and Wandell [26] determines the basis functions by minimizing the errors in the predicted scanner responses. The method described in this paper

assumes that the basis functions are represented by rational Gaussian basis functions and determines the parameters of the basis functions from predicted scanner responses.

5 RESULTS AND DISCUSSION

To evaluate the effectiveness of the proposed geometry and color correction method, the color chart shown in Fig. 1 was used. This is the MacBeth ColorChecker color chart [27]. The color names, along with CIE 1931 color values can be found in [27]. The chart has been used in various applications including standardization of TV monitor colors and copier colors. Because the chart is divided into uniformly spaced and homogeneous color patches of the same size, we used it to correct the geometry as well as the color of an image.

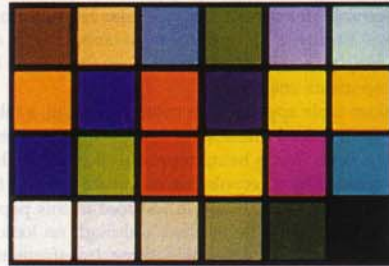


Fig. 1. The MacBeth ColorChecker color chart [27] used to evaluate the proposed geometry and color correction method.

The MacBeth color chart is available in printed form on 8.5×11 inch paper. We placed a printed color chart in front of a Nikon F camera with a Micro-Nikkor lens and obtained images at focal lengths between 50 and 55 mm. The illumination in the scene and the shutter speed of the camera were varied while obtaining the images. Four different light sources (daylight, electronic flash, tungsten, and fluorescent) were used in the experiments, and the shutter speed of the camera was set to five different levels (f stops of $-2, -1, 0, +1,$ and $+2$). Fig. 2 shows images obtained when electronic flash was used with different shutter speeds, while Fig. 3 shows images obtained when a fixed shutter speed (f stop of 0) was kept but the scene illumination was changed. Overall, 20 images of 160×200 pixels each were obtained from all combinations of light sources and shutter speeds.

To determine the geometry correction accuracy of the proposed method, seven patch corners (shown by rectangles in Fig. 4) were used to estimate the transformation functions, and eighteen of the corners (shown by ellipses in Fig. 4) were used to evaluate the geometry correction accuracy. Corners of the color patches to the extreme left and right of the chart were not used because some of them fell outside the acquired images.

The coordinates of the seven corresponding corners in the ideal image (Fig. 1) and each of the 20 images were used to determine the transformation functions for geometry correction. After correcting the geometry of each image, the coordinates of the obtained 18 corners were compared to the coordinates of corresponding corners in the image of Fig. 1. The results of this comparison are shown in Table 1. Mean and Max denote the mean and maximum distances of the 18 corresponding corners in the image of Fig. 1 and in each of the acquired images. As can be observed from the results in Table 1, geometric distortion is not a function of scene illumination and hardly varies with the shutter speed of the camera. The small error variations in different images can be attributed to the fact that not all point correspondences could be determined with the same accuracy. Because of the rather low resolution of our images, we did not observe a significant difference between the errors in the three bands of a color image.

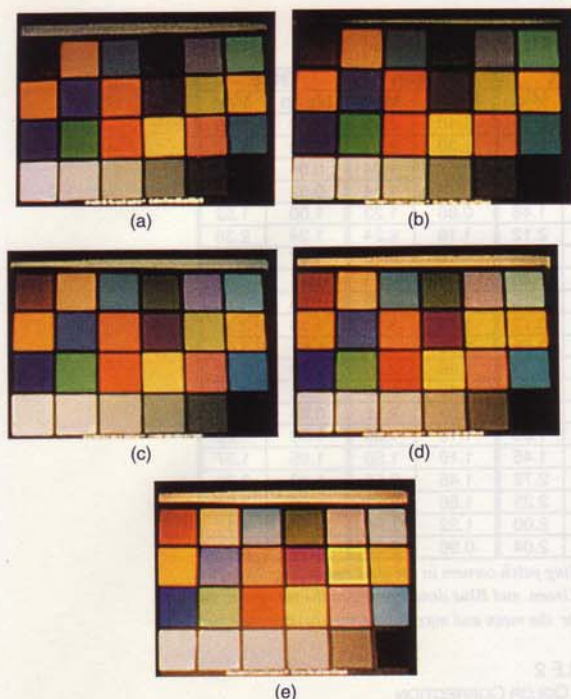


Fig. 2. Image obtained with the same scene illumination (flash light), but with different shutter speeds. The f stops in (a)-(e) were -2 , -1 , 0 , $+1$, and $+2$, respectively.

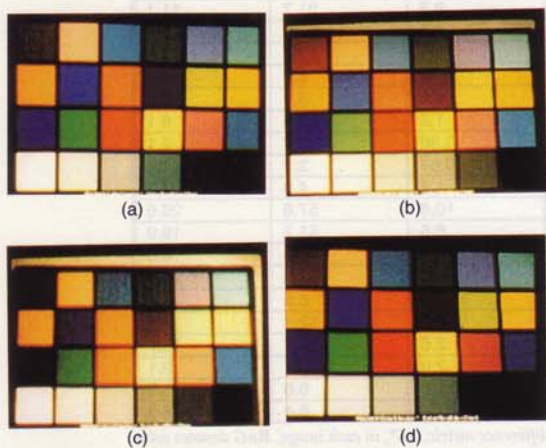


Fig. 3. Images obtained with the same shutter speed (f stop of 0) but with different scene illuminations. Images (a)-(d) were obtained using daylight, electronic flash, tungsten, and fluorescent lighting, respectively.

The errors listed in Table 1 resulted partly from the inability to determine the exact point correspondences. To determine the correspondence between the patch corners in the image of Fig. 1 and the patch corners in each of the 20 images, the approximate positions of corresponding points were first selected manually and then refined by template matching [6]. The algorithm we used refined the point correspondences up to half-a-pixel accuracy. Template matching uses image intensities and becomes inaccurate in the presence of noise. Because corresponding points were first selected manually, the search area chosen for template matching

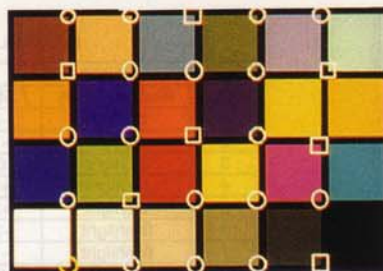


Fig. 4. The corners contained in rectangles are the points used to determine the transformation functions for geometry correction. The corners contained in ellipses are the points used to determine the residual errors in geometry correction.

could be sufficiently small to avoid large mismatches.

It should be mentioned that using a larger number of grid points may not necessarily improve the geometry correction accuracy. Using 14 points, we obtained errors that were similar to those obtained using seven points. If deformation across an image varies smoothly, a few point correspondences are sufficient to correct the geometry of the image satisfactorily.

After correcting the geometry of each color band in each image, we corrected the image colors according to the procedure outlined in Section 4. To determine the transformation functions for color correction, we used half of the color patches. The remaining color patches were used to evaluate the color correction accuracy. Color patches in the first, third, and fifth columns in the color chart were used to determine the transformation functions for color correction, and patches in the second, fourth, and sixth columns were used to measure the accuracy of the color correction.

The color correction errors were computed using the CIE 1976, CIELAB, perceptual color difference measure ΔE^* [22]. To obtain Table 2, an image was segmented into uniform color patches using the recursive thresholding technique of Ohlander et al. [29]. Only the interior pixels of the regions (excluding the boundary pixels) were used. The color of a boundary pixel represents an average of the color of the patch and its background and should not be included in the computations. Once the color patches were identified, the perceptual color difference between the average of each color patch and the value at the corresponding patch in the ideal chart (Fig. 1) was determined. The mean and maximum color differences for each image are reported. The computations were carried out twice, once before correcting an image's color and again after correcting the color of the image according to the procedure outlined in Section 4 with rational Gaussian hypersurfaces of standard deviation equal to 0.025. The results are shown in Table 2 under "RaG."

The entire process was repeated again, this time using rational Gaussian hypersurfaces of standard deviation equal to 0.001. For such a small standard deviation, a rational Gaussian function will behave like a piecewise linear function [8] and, when quantized, will produce values that are similar to those obtained by a piecewise linear function. Therefore, as the standard deviations of Gaussians are decreased, errors obtained by rational Gaussian hypersurfaces will converge to those obtained by piecewise linear functions. Errors obtained with standard deviation equal to 0.001 are shown under "Linear" in Table 2. These results show that color correction using the proposed method produces errors that are, in average, half those obtained by piecewise linear functions.

Due to image noise and inhomogeneous scene illumination, the patches in our images did not have homogeneous colors, and, because the transformation functions used for color correction were determined using the average colors at the patches, some errors still remain after color correction.

TABLE 1
RESIDUAL ERRORS IN GEOMETRY CORRECTION

No.	Image		Red		Green		Blue	
	Illumination	f/Stop	Mean	Max	Mean	Max	Mean	Max
1	daylight	-2	1.33	2.10	1.40	2.20	1.72	2.45
2	daylight	-1	1.44	2.56	1.30	2.41	1.38	2.52
3	daylight	0	1.02	1.53	0.88	1.24	0.94	1.26
4	daylight	+1	0.88	1.62	0.76	1.54	0.92	1.74
5	daylight	+2	0.92	1.48	0.86	1.23	1.00	1.52
6	flashlight	-2	1.12	2.12	1.18	2.24	1.24	2.38
7	flashlight	-1	1.23	2.32	1.18	2.40	1.27	4.41
8	flashlight	0	1.29	2.60	1.43	2.74	1.45	2.73
9	flashlight	+1	1.32	2.15	1.63	2.22	1.48	2.32
10	flashlight	+2	1.66	3.12	1.75	3.17	1.76	3.19
11	tungsten	-2	1.60	3.65	1.55	3.48	1.61	3.61
12	tungsten	-1	1.16	2.13	1.26	2.25	1.20	2.33
13	tungsten	0	1.58	2.98	1.43	2.86	1.63	3.05
14	tungsten	+1	1.00	2.20	1.02	2.12	0.98	2.05
15	tungsten	+2	1.18	1.33	1.10	1.38	1.09	1.28
16	fluorescent	-2	1.12	1.45	1.10	1.50	1.05	1.37
17	fluorescent	-1	1.43	2.72	1.45	2.55	1.40	2.60
18	fluorescent	0	1.67	2.25	1.66	2.33	1.66	2.28
19	fluorescent	+1	1.12	2.00	1.22	1.98	1.16	2.15
20	fluorescent	+2	0.88	2.04	0.96	2.08	1.03	2.23

Table entries show distances in pixels of 18 corresponding patch corners in the ideal image (Fig. 1) and in each of the 20 images after geometry correction. Red, Green, and Blue denote errors in the red, green, and blue bands of a color image, and Mean and Max denote the mean and maximum errors in each color band.

TABLE 2
RESIDUAL ERRORS IN COLOR CORRECTION

Image No.	Before Correction		After Correction			
	Mean	Max	Linear _(Mean)	RaG _(Mean)	Linear _(Max)	RaG _(Max)
1	20.2	40.6	12.5	4.5	37.2	11.6
2	21.9	43.1	7.8	3.3	31.7	11.1
3	19.8	39.2	4.1	1.3	17.0	5.2
4	17.4	37.1	2.0	1.4	8.7	6.6
5	17.8	36.6	2.8	0.91	6.9	3.4
6	18.9	40.9	2.8	1.0	6.9	2.6
7	17.5	41.5	3.6	1.2	10.6	6.1
8	15.9	45.6	3.3	0.86	5.7	2.1
9	19.7	49.2	2.7	0.64	3.2	1.46
10	27.5	57.2	2.9	1.2	4.9	3.1
11	37.6	84.5	12.5	10.8	57.8	26.6
12	29.9	61.7	15.7	6.5	51.2	19.9
13	26.3	55.3	9.9	4.8	47.0	18.0
14	24.8	58.8	5.6	2.7	33.3	15.4
15	23.0	62.3	2.4	1.2	8.8	3.8
16	23.9	68.3	3.1	1.6	12.1	5.5
17	23.6	43.7	5.7	2.6	38.7	15.7
18	17.7	34.5	4.2	2.0	23.2	9.1
19	16.0	32.9	3.5	1.0	6.0	3.0
20	16.2	31.9	1.9	1.2	8.4	3.8

Mean and Max denote the mean and maximum CIELAB color difference metric, ΔE^* , in each image. RaG denotes color correction using the proposed method and Linear denotes color correction using piecewise linear functions. Image numbers in this table are the same as those in Table 1.

A study carried out by Stokes et al. [35] shows that, if CIELAB errors are smaller than two or three, the residual correction errors will not be visible by the eye. Although some errors in Table 2 are larger than two or three, the color correction process has considerably reduced their magnitudes. The maximum errors are larger than three in most images, but the mean errors are mostly less than three. This can be attributed to image noise. Color variations within a patch remain after color correction. The proposed color correction method cannot correct color distortions due to random noise. To reduce errors due to noise, one may average colors in multiple images taken in fast succession.

From Table 2, we see that the worst results are obtained when tungsten lighting (Images 11 through 15) is used. The reason for this is that our camera system was "balanced" to daylight, with maximum sensitivity at 5,400 K. Electronic flash, which produced rather good results, is about 6,000 K and has a spectrum close to that of daylight. Tungsten, however, is about 3,600 K and has quite a different spectrum. This shows that the red, green, and blue filters used in a color camera considerably influence the color correction accuracy. Vrhel and Trussell [39] describe a method for selecting the color filters using a priori knowledge about the scene illumination to improve the color correction accuracy.

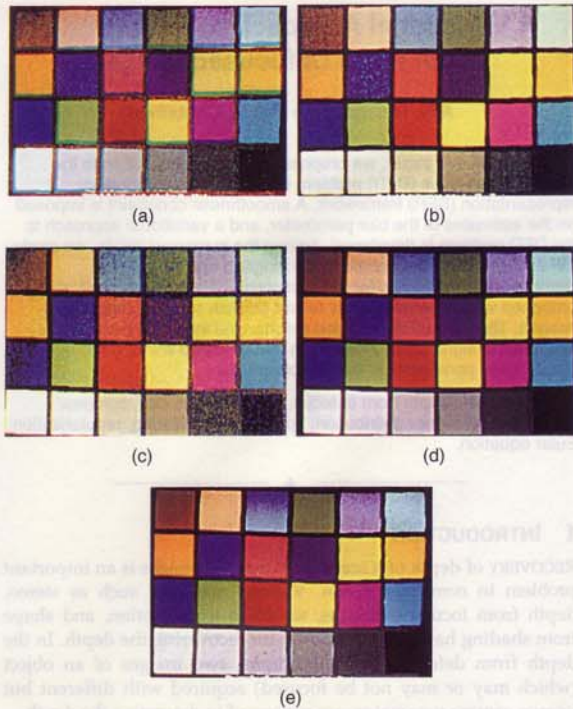


Fig. 5. Images of Fig. 2 after geometry and color correction.

The results of our geometry and color correction method on images of Figs. 2 and 3 are shown in Figs. 5 and 6. The nearest-neighbor resampling method was used to obtain these images. To visually evaluate the quality of our geometry and color correction method, images in Figs. 5 and 6 should be compared with the image in Fig. 1.

6 CONCLUDING REMARKS

In many vision applications, objects in a scene are recognized by their shapes, sizes, and colors. In order to produce consistent results by a vision system, it is necessary to standardize the images so that they contain as little geometry and color distortions as possible. Because it is not possible to acquire images that are free of geometry and color distortions, a preprocessing operation was proposed to transform the acquired images to standard images obtained by an ideal camera in an ideal environment.

A unified method for correcting the geometry and color of digital images was introduced. This method uses a color chart with a known array of color patches. Rational Gaussian surfaces were used as transformation functions to characterize the geometry and color characteristics of the image acquisition system. Experimental results show that the proposed method can effectively correct an image's geometry and color under a variety of camera and illumination settings. Experimental results also show that, although the power of the light source or the shutter speed of the camera do not affect the geometry correction accuracy, they influence the color correction accuracy considerably.

ACKNOWLEDGMENTS

We would like to thank the U.S. National Science Foundation for supporting this work under grants IRI-9529045 and IRI-9509253. We also would like to thank the anonymous reviewers for their insightful comments and suggestions.

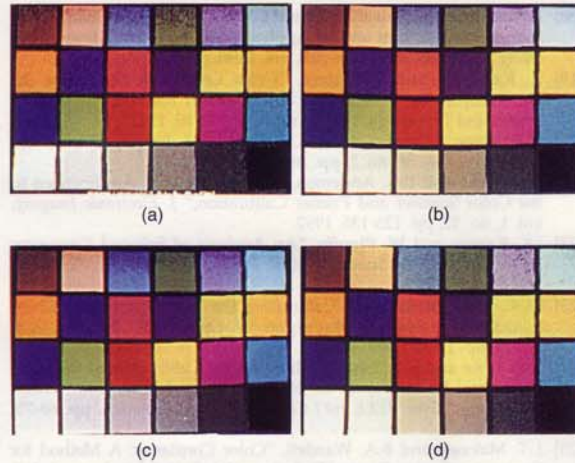


Fig. 6. Images of Fig. 3 after geometry and color correction.

REFERENCES

- [1] K. Barnard, G. Finlayson, and B. Funt, "Colour Constancy for Scenes with Varying Illumination," *Proc. Fourth European Conf. Computer Vision*, vol. II, pp. 3-15, Apr. 15-18, 1996.
- [2] W.B. Cowan, "An Inexpensive Scheme for Calibration of a Color Monitor in Terms of CIE Standard Coordinates," *Computer Graphics*, vol. 17, no. 3, pp. 315-321, 1983.
- [3] J. Duchon, "Splines Minimizing Rotation-Invariant Semi-Norm in Sobolev Spaces," *Constructive Theory of Functions of Several Variables*, W. Schempp and K. Zeller, eds., pp. 85-100. Berlin: Springer-Verlag, 1977.
- [4] T. Echigo, "A Camera Calibration Technique Using Three Sets of Parallel Lines," *Machine Vision and Applications*, vol. 1, no. 3, pp. 159-167, 1990.
- [5] J.G. Fryer and D.C. Brown, "Lens Distortion for Close-Range Photogrammetry," *Photogrammetric Eng. and Remote Sensing*, vol. 52, no. 1, pp. 51-58, 1986.
- [6] A. Goshtasby, S. Gage, and J. Bartholic, "A Two-Stage Cross-Correlation Approach to Template Matching," *IEEE Trans. Pattern Analysis and Machine Intelligence*, vol. 6, no. 3, pp. 374-378, Mar. 1984.
- [7] A. Goshtasby, "Correction of Image Deformation from Lens Distortion Using Bézier Patches," *Computer Vision, Graphics, and Image Processing*, vol. 47, pp. 385-394, 1989.
- [8] A. Goshtasby, "Design and Recovery of 2D and 3D Shapes Using Rational Gaussian Curves and Surfaces," *Int'l J. Computer Vision*, vol. 10, no. 3, pp. 233-256, 1993.
- [9] A. Goshtasby and W.D. O'Neill, "Surface Fitting to Scattered Data by a Sum of Gaussians," *Computer Aided Geometric Design*, vol. 10, pp. 143-156, 1993.
- [10] A. Goshtasby, "Geometric Modeling Using Rational Gaussian Curves and Surfaces," *Computer-Aided Design*, vol. 27, no. 5, pp. 363-375, 1995.
- [11] W.B. Green, P.L. Jespen, J.E. Kreznar, R.M. Ruiz, A.A. Schwartz, and J.B. Seidman, "Removal of Instrument Signature from Mariner 9 Television Images of Mars," *Applied Optics*, vol. 14, no. 1, pp. 105-114, 1975.
- [12] R.L. Hardy, "Theory and Applications of the Multiquadric-Biharmonic Method," *Computer Math. Applications*, vol. 19, nos. 8/9, pp. 1,905-1,915, 1990.
- [13] G. Healey and D. Slater, "Global Color Constancy: Recognition of Objects by Use of Illumination-Invariant Properties of Color Distributions," *J. Optical Soc. Am.*, vol. A-11, no. 11, pp. 3,003-3,010, 1994.
- [14] R. Holub, W. Kearsley, and C. Pearson, "Color Systems Calibration for Graphics Arts: I. Input Devices," *J. Imaging Technology*, vol. 14, no. 2, pp. 47-52, 1988.
- [15] R. Holub, W. Kearsley, and C. Pearson, "Color Systems Calibration for Graphics Arts: II. Output Devices," *J. Imaging Technology*, vol. 14, no. 2, pp. 53-60, 1988.
- [16] P.-C. Hung, "Color Rendition Using Three-Dimensional Interpolation," *Proc. SPIE: Imaging Applications in the Work World*, pp. 111-115, 1988.
- [17] P.-C. Hung, "Colorimetric Calibration for Scanners and Media," *Proc. SPIE: Camera and Input Scanner Systems*, vol. 1,448, pp. 164-174, 1991.

- [18] K. Kanamori, H. Kawakami, and H. Kotera, "A Novel Color Transformation Algorithm and Its Applications," *Proc. SPIE: Image Processing Algorithms and Techniques*, vol. 1,244, pp. 272-281, 1990.
- [19] K. Kanamori and H. Kotera, "Color Correction Technique for Hard Copies by 4-Neighbors Interpolation Method," *J. Imaging Science and Technology*, vol. 36, no. 1, pp. 73-80, 1992.
- [20] H.R. Kang, "Color Scanner Calibration," *J. Imaging Science and Technology*, vol. 36, no. 2, pp. 162-170, 1992.
- [21] R.H. Kang and P.G. Anderson, "Neural Network Applications to the Color Scanner and Printer Calibration," *J. Electronic Imaging*, vol. 1, no. 12, pp. 125-135, 1992.
- [22] J.K. Kasson and W. Plouffe, "An Analysis of Selected Computer Interchange Color Spaces," *ACM Trans. Graphics*, vol. 11, no. 4, pp. 373-405, 1992.
- [23] H.-C. Lee, "Method for Computing the Scene-Illuminant Chromaticity from Specular Highlights," *J. Optical Soc. Am.*, vol. A-3, no. 10, pp. 1,694-1,699, 1986.
- [24] R.K. Lenz and R.Y. Tsai, "Techniques for Calibration of the Scale Factor and Image Center for High Accuracy 3-D Machine Vision Metrology," *Proc. IEEE Int'l Conf. Robotics Automation*, pp. 68-75, Mar. 1987.
- [25] L.T. Maloney and B.A. Wandell, "Color Constancy: A Method for Recovering Surface Spectral Reflectance," *J. Optical Soc. Am.*, vol. A-3, no. 1, pp. 29-33, 1986.
- [26] D.H. Marimont and B.A. Wandell, "Linear Models of Surface and Illuminant Spectra," *J. Optical Soc. Am.* vol. A-9, no. 11, pp. 1,906-1,913, 1992.
- [27] C.S. McCamy, H. Marcus, and J.G. Davidson, "A Color-Rendition Chart," *J. Applied Photographic Eng.*, vol. 2, no. 3, pp. 95-99, 1976.
- [28] M. Nagao, T. Matsuyama, and Y. Ikeda, "Region Extraction and Shape Analysis in Aerial Photographs," *Computer Graphics and Image Processing*, vol. 10, pp. 195-223, 1979.
- [29] R. Ohlander, K. Price, and R. Reddy, "Picture Segmentation Using a Recursive Region Splitting Method," *Computer Graphics and Image Processing*, vol. 8, pp. 313-333, 1978.
- [30] P.S. Parkkinen, J. Hallikainen, and T. Jaaskelainen, "Characteristic Spectra of Munsell Colors," *J. Optical Soc. Am.* vol. A-6, pp. 318-322, 1989.
- [31] M.J.D. Powell, "Radial Basis Functions for Multivariate Interpolation: A Review," *Algorithms for Approximation*, J.C. Mason and M.G. Cox, eds., pp. 143-167. Oxford: Clarendon Press, 1987.
- [32] A. Sai, S.M. Bloor, and A. Pennington, "Sculptured Solids in CSG-Based Geometric Modeling System," *The Mathematics of Surfaces II*, R.R. Martin, ed., pp. 321-341. Oxford Univ. Press, 1987.
- [33] K. Staes, "Light Sources as an Integral Part of the Color Photographic System," *Soc. Motion Picture and Television Eng. J.*, vol. 86, pp. 537-543, 1997.
- [34] M. Swain and D. Ballard, "Color Indexing," *Int'l J. Computer Vision*, vol. 7, pp. 11-32, 1991.
- [35] M. Stokes, M.D. Fairchild, and R.S. Berns, "Precision Requirements for Digital Color Reproduction," *ACM Trans. Graphics*, vol. 11, no. 4, pp. 406-422, 1992.
- [36] M. Thompson, *Manual of Photogrammetry*, third edition, pp. 84-86. Washington, D.C.: Am. Soc. Photogrammetry, 1976.
- [37] R.Y. Tsai, "An Efficient and Accurate Camera Calibration Technique for 3D Machine Vision," *Computer Vision, Graphics, and Image Processing*, vol. 3, no. 4, pp. 346-374, 1986.
- [38] M.J. Vrhel and H.J. Trussell, "Color Correction Using Principal Components," *Color Research and Application*, vol. 17, no. 5, pp. 328-338, 1992.
- [39] M.J. Vrhel and H.J. Trussell, "Filter Consideration in Color Correction," *IEEE Trans. Image Processing*, vol. 3, no. 2, pp. 147-161, 1994.
- [40] L.-L. Wang and W.-H. Tsai, "Camera Calibration by Vanishing Lines for 3D Computer Vision," *IEEE Trans. Pattern Analysis and Machine Intelligence*, vol. 14, no. 10, pp. 965-980, Oct. 1992.
- [41] J. Weng, P. Cohen, and M. Herniou, "Camera Calibration with Distortion Models and Accuracy Evaluation," *IEEE Trans. Pattern Analysis and Machine Intelligence*, vol. 14, no. 10, pp. 965-980, Oct. 1992.
- [42] R.G. Willson, "Modeling and Calibration of Automated Zoom Lenses," PhD dissertation, Technical Report #CMU-RI-TR-94-03, Carnegie Mellon Univ., Jan. 1994.

A Variational Approach to Recovering Depth From Defocused Images

A.N. Rajagopalan and S. Chaudhuri

Abstract—In this paper, we propose a regularized solution to the depth from defocus (DFD) problem using the space-frequency representation (SFR) framework. A smoothness constraint is imposed on the estimates of the blur parameter, and a variational approach to the DFD problem is developed. Among the numerous SFRs, we study the applicability of the complex spectrogram and the Wigner distribution, in particular, for depth recovery. The performance of the proposed variational method is tested on both synthetic and real images. The method yields good results, and the quality of the estimates is significantly better than that obtained without the smoothness constraint on the blur parameter.

Index Terms—Depth from defocus, space-variant blur, complex spectrogram, Wigner distribution, space-variant filtering, regularization, Euler equation.

1 INTRODUCTION

RECOVERY of depth of a scene from a set of images is an important problem in computer vision. Various methods, such as stereo, depth from focus or defocus, structure from motion, and shape from shading have been proposed for recovering the depth. In the depth from defocus (DFD) technique, two images of an object (which may or may not be focused) acquired with different but known camera parameters are processed to determine the depth.

In previous work related to DFD, Pentland [1] compared two images of a scene, one formed with a very small (pin-hole) aperture, and the other image formed with a normal aperture. By approximating the camera defocus blur by the Gaussian function, the depth was recovered through inverse filtering. In [2], Subbarao proposed a more general method that allows several camera parameters to be varied simultaneously. Hwang et al. estimate the blur parameter using a differential algorithm in the spatial domain [3]. Bove [4] poses the problem as one of signal estimation and estimates the parameters of the defocusing process. In [5], Ens and Lawrence propose a matrix-based approach to the DFD problem. In [6], Xiong and Shafer suggest an iterative blur estimation scheme to reduce the error due to windowing. Pentland et al. introduce the notion of active depth from defocus [7] in which the apparent blurring of a known pattern of light is measured to estimate the depth. In [8], Gökstorp estimates blur by obtaining local estimates of instantaneous frequency, amplitude, and phase using a set of Gabor filters in a multiresolution framework. Xiong et al. suggest a Gabor filter-based variable window scheme [9] that demonstrates a greater flexibility and a better adaptability to image contents as compared to the fixed-window-size scheme. Recently, Rajagopalan and Chaudhuri have proposed a block shift-variant blur model for recovering the depth [10]. The DFD technique has been used for image recovery in [11]. In [12], Nayar et al. describe a real-time range focus sensor that uses an optimized illumination pattern to obtain accurate and high-resolution depth

- The authors are with the Department of Electrical Engineering, Indian Institute of Technology-Bombay, Powai, Bombay, 400 076, India. E-mail: {raju,sc}@ee.iitb.ernet.in.

Manuscript received 10 Apr. 1996; revised 7 Aug. 1997. Recommended for acceptance by S.K. Nayar.

For information on obtaining reprints of this article, please send e-mail to: tpami@computer.org, and reference IEEECS Log Number 105506.